Measuring measurement

J.S. Lundeen[1],[*] A. Feito[2,3], H. Coldenstrodt-Ronge[1], K.L. Pregnell[2,3], Ch.
Silberhorn[4], T.C. Ralph[5], J. Eisert[2,3,6], M.B. Plenio[2,3], and I.A. Walmsley[1]

[1]*Clarendon Laboratory, Oxford University, Parks Road, Oxford, OX1 3PU, UK*
[2]*Institute for Mathematical Sciences, Imperial College London, SW7 2PE, UK*
[3]*QOLS, The Blackett Laboratory, Imperial College London, Prince Consort Rd., SW7 2BW, UK*
[4]*Max-Planck Research Group for Optics, Information and Photonics, Erlangen, Germany*
[5]*Department of Physics, University of Queensland, Brisbane, QLD 4072, Australia and*
[6]*Institute for Physics and Astronomy, University of Potsdam, 14476 Potsdam, Germany*
(Dated: July 15, 2008)

Measurement connects the world of quantum phenomena to the world of classical events. It plays both a passive role, observing quantum systems, and an active one, preparing quantum states and controlling them. Surprisingly – in the light of the central status of measurement in quantum mechanics – there is no general recipe for designing a detector that measures a given observable [1]. Compounding this, the characterization of existing detectors is typically based on partial calibrations or elaborate models. Thus, experimental specification (i.e. tomography) of a detector is of fundamental and practical importance. Here, we present the realization of quantum detector tomography [2–4]: we identify the optimal positive-operator-valued measure describing the detector, with no ancillary assumptions. This result completes the triad, state [5–11], process [12–17], and detector tomography, required to fully specify an experiment. We characterize an avalanche photodiode and a photon number resolving detector capable of detecting up to eight photons [18]. This creates a new set of tools for accurately detecting and preparing non-classical light.

Von Neumann's postulate of the reduction of the quantum state by measurement is now generally accepted to be a limiting case of a more general theory of quantum measurement. However, even within this general theory it is not known how to incorporate the complete chain of apparatus components in a derivation of the actual measurement: Braginsky wrote, "the Schrödinger equation cannot tell us the connection between the design of the measuring device and the nature of the measurement [1]." Measurement is increasingly becoming a driving component in quantum technologies such as super-resolution metrology [19], Heisenberg-limited sensitivity [20], and quantum computing [21]. Input states and dynamical processes are accepted as resources for quantum technologies and therefore the techniques of quantum state tomography (QST) [5–11] and quantum process tomography (QPT) [12–17] have been developed to measure them. A distinct omission is that of the experimental tomography of detectors, which would enable more accurate classification of measurement types, objective comparison of competing devices, and precise design of new detectors. This omission is even more striking given that the tomography of states and processes are predicated on a well characterized detector. In this paper, we extend previous theoretical descriptions of detector tomography [2–4] and, by means of efficient numerics based on convex optimization [22] we characterize two quantum detectors.

Characterizing a detector consists of determining its corresponding *positive operator valued measure* (POVM). Given an input state ρ, the probability $p_{n,\rho}$ of obtaining detection outcome n is

$$p_{n,\rho} = \mathrm{tr}[\rho\, \pi_n], \qquad (1)$$

where $\{\pi_n\}$ is the detector POVM. In state tomography, an unknown ρ is characterized by performing a set of known measurements, each on many identical copies of the state in order to estimate p_n. From this estimate one can invert equation (1) to find ρ. The interchangeability of ρ and π_n in equation (1) shows that detector tomography plays a dual role to state tomography. Now, measuring a set of known probe states $\{\rho\}$ allows us to characterize an unknown detector, and thus find $\{\pi_n\}$. For these operators to describe a physical measurement apparatus, they must be positive semi-definite, $\pi_n \geq 0$, and $\sum_n \pi_n = I$, ensuring positive probabilities that add up to one. In addition, the operators $\{\rho\}$ must be chosen to be *tomographically complete*, i.e. form a basis for the operator space of π_n.

In the specific case of optical detectors, lasers provide us with an ideal tomographic probe: the coherent state $|\alpha\rangle$. By transforming the magnitude $|\alpha|$ through attenuation (e.g. with a beamsplitter) and the phase $\arg(\alpha)$ by optical delay, we can create a tomographically complete set of probe states $\{|\alpha\rangle\langle\alpha|\}$ (the existence of the P-function is a proof of completeness). Remarkably, with coherent state probes, the measured statistics are themselves a full representation of the detector in the form of the Q-function [2],

$$Q_n(\alpha) = \frac{1}{\pi}\langle\alpha|\pi_n|\alpha\rangle = \frac{1}{\pi}p_{n,\alpha}. \qquad (2)$$

Since $Q_n(\alpha)$ of each POVM element contains the same information as the element π_n itself, this is already detector tomography. Predictions of the detection probabilities for arbitrary input states can then be calculated directly from the Q-function representation. Unfortunately, experimental errors and statistical fluctuations can cause a simple fit to the Q-function to be consistent with unphysical POVM elements. Due to this we ultimately wish to directly find the POVM el-

ements $\{\pi_n\}$ that are closest to the measured statistics, while constraining them to be physical.

We now turn to the description of the experimental realization, shown in Fig. 2 (see methods). The first detector was a commercial single-photon counting module based on a silicon avalanche photodiode (APD). It has two detection outcomes, either outputting an electronic pulse (1-click) or not (0-clicks). Past evaluation of the detector has shown that the 1-click outcome is mainly associated with the arrival of one or more photons, although dark counts and afterpulsing can also create this outcome. The 0-click event is mainly associated with vacuum at the input or photons lost due to non-unit efficiency of the photodiode. Having only two outcomes, this detector cannot directly measure the incoming photon number if it is above one. The second detector circumvents this by splitting the incoming pulse into many spatially or temporally separate bins, making unlikely the presence of more than one photon per bin. Subsequently all the bins are detected with two APDs. Photon-number resolution results by summing the number of 1-click outcomes from all the bins. This *time-multiplexed detector* (TMD) is not commercially available but can be constructed with standard tools [18]. Ours has eight bins in total (four time bins in each of two output fibres) and thus nine outcomes – from zero to eight clicks, making it capable of detecting up to eight photons. The added complexity and greater number of outcomes of this detector provide a more challenging test for detector tomography.

For both detectors we first allowed the phase of α to drift. We observed no variation in the outcome frequencies, as expected from a detector without a phase-reference. This simplifies the experimental procedure, requiring us to control only the magnitude of α (as has been done for tomography of a single photon [23]). A detector with no observed phase dependence will be described by POVM elements diagonal in the number basis,

$$\pi_n = \sum_{k=0}^{\infty} \theta_k^{(n)} |k\rangle\langle k|, \tag{3}$$

simplifying henceforth the reconstruction of π_n.

For a POVM set $\{\pi_n\}$ containing only diagonal matrices that are each truncated at a number state M, we can rewrite equation (2) as a matrix equation,

$$P = F\,\Pi. \tag{4}$$

For an N outcome detector, $P_{D \times N}$ contains all the measured statistics, $F_{D \times M}$ contains the D probe states $\alpha, \alpha_1, \ldots, \alpha_D$, and $\Pi_{M \times N}$ contains the unknown POVM set (matrix subscripts are the matrix dimensions). For a coherent state probe, $F_{i,k} = |\alpha_i|^{2k} \exp\left(-|\alpha_i|^2\right)/k!$. This can easily be reformulated for a probe in a mixed state, as was done to model the laser technical noise (see methods). The optimal physical POVM consistent with the data can be estimated through
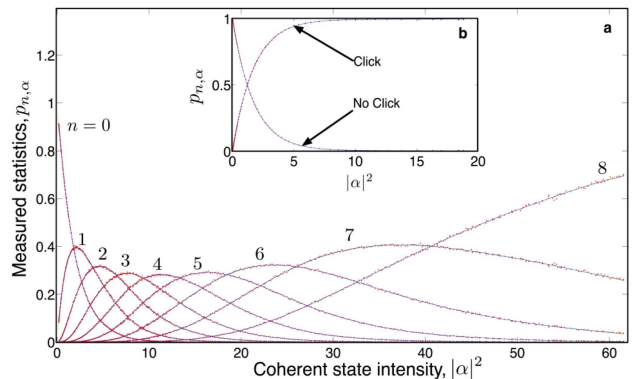

FIG. 1: The detector tomography data. The outcome statistics (red dots) are measured as a function of the coherent state magnitude $|\alpha|^2$ and form an estimate of $p_{n,\alpha}$ for each detector outcome n (number of clicks). Since they are proportional to the Q-function $Q_n(\alpha)$ for each outcome, the statistics directly fully characterize the detector. The main plot corresponds to time multiplexed detector (TMD) with nine outcomes and the inset corresponds to the avalanche photodiode (APD). The vertical statistical error is too small to be seen. From the reconstructed POVM elements $\{\pi_n\}$ we generate the corresponding probabilities $p_{n,\alpha} = \langle\alpha|\pi_n|\alpha\rangle$ (blue curves).
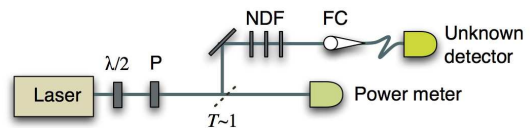

FIG. 2: The experimental setup. A half-waveplate ($\lambda/2$) and Glan-Thompson polarizer (P) are used to vary the amplitude of the probe coherent state, which is subsequently attenuated by Neutral Density Filters (NDF) and coupled into a fibre (FC) (see methods for more details).

the following optimization problem:

$$\min\left\{||P - F\Pi||_2 + g(\Pi)\right\},$$

$$\text{subject to} \quad \pi_n \geq 0, \quad \sum_{n=0}^{N-1} \pi_n = I, \tag{5}$$

where the 2-norm of a matrix A is defined as $||A||_2 = \left(\sum_{i,j} |A_{i,j}|^2\right)^{1/2}$. Note that we allow for regularization in the form of convex quadratic functions g, related to the conditioning of the problem, which must not depend on the type of detector. This is a convex quadratic optimization problem, and hence also a semi-definite problem (SDP) [22] which can be efficiently solved numerically. Moreover, in this case, there exists a dual optimization problem whose solution coincides with the original problem. Thus, the dual problem provides a certificate of optimality that we use to verify our solution.

The measured statistics for each detector outcome (i.e. number of clicks) are shown in Fig. 1 for the TMD and for the APD. The distributions (equivalent to the Q-function $Q_n(\alpha)$ of the detector) show smooth profiles and distinct photon number ranges of sensitivity for increasing number of *clicks* in the detector. Fig. 3 shows the diagonals (the off-diagonals
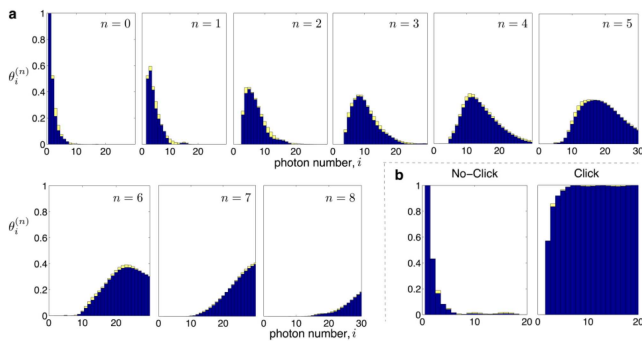
FIG. 3: The optimal physical POVMs. We present the diagonals of the reconstructed POVMs represented in the photon-number basis for (a) the photon-number resolving TMD and (b) the binary APD detector. The TMD POVM elements were obtained up to basis state $|60\rangle\langle60|$ (therefore $M = 60$), but are shown up to $|30\rangle\langle30|$ for display purposes. The APD POVM elements are shown in full. Stacked on top of each $\theta_i^{(n)}$ we show $|\theta_i^{(n)(\mathrm{rec})} - \theta_i^{(n)(\mathrm{teo})}|$ in yellow, where n is the number of clicks, and rec and teo are the reconstructed and theoretical diagonals of POVM element, π_n. The theoretical TMD and APD models are described in methods.

are zero for these phase insensitive detectors) of the POVMs that result from optimization of equation (5) (see methods for $g(\Pi)$). Note that π_n, being the POVM element for n clicks, shows nearly zero amplitude for detecting less than n photons, exhibiting essentially no dark counts. Prominent in an otherwise smooth distribution, this sharp feature provides the detector with its discriminatory power: n clicks guarantees there were at least n photons in the input pulse. To assess the performance of the tomography we find the difference (yellow bars in Fig. 3) between the estimated POVM elements π_n^{rec} and a previously developed simple theoretical model of a TMD, π_n^{teo} [24] (see methods). The fidelity

$$F = \mathrm{tr}\left(\left(\sqrt{\pi_n^{\mathrm{teo}}}\pi_n^{\mathrm{rec}}\sqrt{\pi_n^{\mathrm{teo}}}\right)^{\frac{1}{2}}\right)^2 \geq 98.7\%$$

for all n, indicating excellent agreement between the two.

To visualize the action of the detector, in the special case of optical detectors one can plot a Wigner function of each of the reconstructed POVM elements, $W_n(\alpha, \alpha^*)$. The response of the detector to an input state with Wigner function W_ψ is proportional to the overlap,

$$p_{n,\psi} = \int W_n W_\psi d\alpha d\alpha^*.$$

We focus on the one click Wigner function $W_1(\alpha, \alpha^*)$ for the APD (Fig. 4a) and the TMD (Fig. 4b). An APD detector is sometimes regarded as a 'single photon detector' but here we can see the marked difference between the two Wigner functions. Instead, it is the TMD that has a fidelity of 98% with a single photon (having experienced a 52.2% loss). Conversely, the APD Wigner function extends to $\alpha \gg 1$, having significant overlap with photon number states ≥ 1. Therefore, to use an APD as a 'single photon detector' one must make
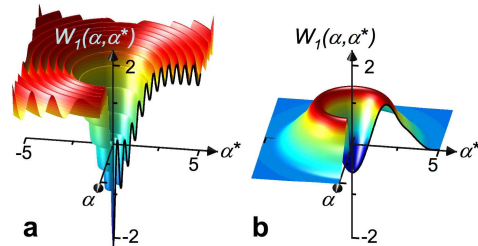

FIG. 4: The Wigner functions of the 'one click' detector outcomes. From the diagonal elements of π_1 for the APD (a) and TMD (b) one can generate the Wigner function representing their measurement of the optical mode.

the ancillary assumption that the input beam has insignificant components containing more than one photon. Despite their differences, both Wigner functions have negative values near the origin, indicating the absence of a classical optical analogue. Consequently, these are both fundamentally quantum detectors.

As quantum technologies advance, detectors are becoming more complex, making a black-box approach to their characterization an important tool. Identifying the exact operations of detectors will benefit precision tasks, such as state tomography or metrology. By eliminating assumptions, full characterization enables more flexible design and use of detectors, be they noisy, nonlinear, inefficient, or operating outside their normal range. With precise characterization we can ask precise quantitative questions about our power to prepare non-classical states or herald quantum operations [21]. This opens a path for the experimental study of yet unexplored concepts such as the non-classicality of detectors. For optical detector tomography, a promising avenue for research will be to transfer well-established techniques from homodyne tomography (e.g. balanced noise-reduction, direct measurement of the Wigner function or pattern functions [25]). Now that it is well characterized, the photon counter also provides a unique tool for performing non-Gaussian operations, which are critical for quantum information processing using the electromagnetic field as the information carrier [26, 27]. As superconducting and semiconductor photon number counters are developed, tomography could be used as an objective benchmark to compare competing devices. Moreover, for one of these photon number counters only an incomplete and empirical model is available [28], making detector tomography the best option to completely determine its action. We expect detector tomography will become the standard for the adequate calibration of all measurement and state preparation devices.

Methods

Experimental setup

The pulses of a mode-locked laser travel through a half-waveplate ($\lambda/2$) and a Glan-Thompson polarizer (P) with which we varied their amplitude α. We subsequently sent the pulses through a beamsplitter (BS) ($T = 95\%$). The reflected beam travelled through three neutral density (i.e. spectrally flat) filters (NDF) before being coupled into a single-mode fiber (FC). The attenuation from all elements, the reflection off the beamsplitter, each of the filters, and fibre-coupling, were measured individually with a calibrated power meter, resulting in a total attenuation γ. This power meter was then placed in the transmission port of the beamsplitter so that the magnitude of α for the probe state in the fibre was found from P, the measured time-averaged power and the pulse rate R via $|\alpha|^2 = \gamma P \lambda / (2\pi R \hbar c)$. For each value of α we recorded the number of times each detection outcome occurred in J trials (i.e. laser pulses), which provides an estimate of $p_{n,\alpha}$.

Source of light and technical noise

The input states were generated by a mode-locked Ti:Sapph laser with center wavelength λ and a FWHM bandwidth of $\Delta\lambda$ specifically chosen for each detector. It was cavity dumped to reduce its repetition rate R in order to be compatible with tested detectors. Long term drift of the intensity over 1 million pulses was $< 0.5\%$. To characterize it, a NIST calibrated Coherent FieldMaxII-TO power meter was used (systematic error of 5%). In the case of the APD detector (a Perkin Elmer SPCM-AQR-13-FC) we set $\lambda = 780 \pm 1$ nm, $\Delta\lambda = 20$ nm, and chose the appropriate rate $R = 1.4975 \pm 0.0005$ kHz, $J = 1472967$, and $\gamma = (5.66 \pm 0.08) \times 10^{-9}$. For the TMD detector we set $\lambda = 789 \pm 1$ nm, $\Delta\lambda = 26$ nm, $R = 76.169 \pm 0.001$ kHz, $J = 38084$, and $\gamma = (8.51 \pm 0.11) \times 10^{-9}$. We now evaluate the importance to our tomography of the technical noise found at some level in all lasers. Our laser randomly varies in energy between subsequent pulses with a standard deviation of $1.88\% \pm 0.02\%$ of $|\alpha|^2$. Attenuated to the signal photon level, as in this experiment, one might expect the inherent large fractional uncertainty in the coherent state to render this technical noise insignificant. We test this expectation by modelling the pulse distribution as a Gaussian $f_\alpha(\beta) = e^{-(\beta-\alpha)^2/(2\sigma^2)}/(\sigma\sqrt{2\pi})$ centered around α in phase space, with a variance approximately equal to that measured, $\sigma^2 = 0.0004 |\alpha|^4$. Each probe state is then best described by a mixture of coherent states,

$$\rho_{\langle\alpha\rangle} = \int d^2\beta |\beta\rangle\langle\beta| f_\alpha(\beta) \qquad (6)$$

$$= \sum_{l,m=0}^{\infty} E_{l,m,\alpha} |l\rangle\langle m|, \qquad (7)$$

where

$$E_{j,m,\alpha} = \frac{1}{\sigma\sqrt{2\pi}\sqrt{l!m!}} \int \beta^{l+m} e^{-\beta^2 - (\beta-\alpha)^2/(2\sigma^2)} \ d\beta.$$

The detection probability for outcome n is then

$$p_{\langle\alpha\rangle,n} = \sum_{k=0}^{\infty} E_{k,k,\alpha} \theta_k^{(n)}. \qquad (8)$$

Comparing our analysis done with pure input states $|\alpha\rangle\langle\alpha|$ to that done with mixed states $\rho_{\langle\alpha\rangle}$ we find the difference between the POVMs obtained was negligible. For example

$$\frac{||\Pi_{\text{pure}} - \Pi_{\text{mixed}}||_2}{||\Pi_{\text{mixed}}||_2} \leq 0.7\%$$

and the largest relative difference between any two $\theta_k^{(n)}$ coming from a mixed state or a pure state derivation was 1.3%. Furthermore the reconstructed probability distributions are so close that they are indistinguishable on the scale of Fig. 1. This reinforces our earlier expectation that technical noise in the laser will be negligible when using single-photon-level coherent states. This differs from homodyne tomography where technical noise can shift a strong local oscillator to a nearly orthogonal state.

Discussion of regularization

Care has to be taken that the optimization problem is well conditioned in order to find the true POVM of the detector. In finding the number basis representation we are deconvolving a coherent state from our statistics, which is intrinsically an ill-conditioned problem. Similar issues of conditioning have been discussed in the context of state and process tomography, see e.g. Refs. [29, 30]. Due to a large ratio between the largest and smallest singular values of the matrices defining the quadratic problem, small fluctuations in the probability distribution can result in large variations for the reconstructed POVM. This can result in operators that closely approximate the outcome statistics and yet contain errant spikes in their distribution in photon-number. To suppress this effect, we penalize the difference $\theta_k^{(n)} - \theta_{k+1}^{(n)}$ (independent of the shape of the POVM) by using the regularization $g = y\mathcal{S}$ with $\mathcal{S} = \sum_{k,n}[\theta_k^{(n)} - \theta_{k+1}^{(n)}]^2$. This is motivated by the fact that any realistic detector will have a finite efficiency η, which necessitates a smooth $\theta_k^{(n)}$ distribution: if $G(r)$ is the probability of registering r photons and $H(q)$ is the probability that q were present then,

$$G(r) = \sum_q \binom{q}{r} \eta^r (1-\eta)^{q-r} H(q).$$

Consequently, if $\theta_k \neq 0$ then θ_{k+1}, θ_{k+2} etc. cannot be zero, but will follow some smooth distribution. Since we do not assume any knowledge about the precise loss of our detector

we simply choose an arbitrary value for y. Varying y by three orders of magnitude hardly affects the exact value of the estimated POVM, changing it by only 10%. Furthermore, the regularization $g = y\,\mathcal{S}$ also proves to be robust to noise up to $\delta = 0.2$ (varying $\alpha \to \alpha(1+\delta)$ across $\{|\alpha\rangle\langle\alpha|\}$ with a Gaussian distribution for δ). This shows that the regularization's main effect is to suppress the ill-conditioning and noise while leaving the POVM fitting unaffected.

The theoretical model of the detector

The detector tomography does not make use of any physical model on the functioning of the detector. To verify the success of this approach we have compared the outcome of the estimation with those POVM elements obtained from a theoretical model of the APD and TMD [24]. The APD is treated as a binary detector with a loss of 43.2%. The theoretical TMD assumes: No dark counts, three sequential beam splitters with experimentally inferred reflectivities, 50.18%, 50.60%, and 41.92%, and an overall loss of 52.2% (that best fits the data), followed by two perfect APDs.

ACKNOWLEDGEMENTS

COMPETING FINANCIAL INTERESTS STATEMENT

The authors have no competing interests as defined by Nature Publishing Group, or other interests that might be perceived to influence the results and/or discussion reported in this paper.

---

* Electronic address: j.lundeen1@physics.ox.ac.uk

[1] V. R. Braginsky and F. Ya. Khalili, *Quantum measurement*, p. 38 (Cambridge University Press, Cambridge,1992).

[2] Luis, A. & Sanchez-Soto, L. L. Complete characterization of arbitrary quantum measurement processes. Phys. Rev. Lett. **83,** 3573-3576 (1999).

[3] Fiurasek, J. Maximum-likelihood estimation of quantum measurement. Phys. Rev. A **64,** 024102 (2001).

[4] D'Ariano, G.M., Maccone, L. & Presti, P. L. Quantum calibration of measurement instrumentation. Phys. Rev. Lett. **93,** 250407 (2004).

[5] Vogel, K. & Risken, H. Determination of quasiprobability distributions in terms of probability distributions for the rotated quadrature phase. Phys. Rev. A **40,** 2847-2849 (1989).

[6] Smithey, D. T., Beck, M., Raymer, M. G. & Faridani, A. Measurement of the Wigner distribution and the density matrix of a light mode using optical homodyne tomography: Application to squeezed states and the vacuum. Phys. Rev. Lett. **70,** 1244 (1993).

[7] Banaszek, K., Radzewicz, C., Wodkiewicz, K. & Krasinski, J. S. Direct measurement of the Wigner function by photon counting. Phys. Rev. A **60,** 674 (1999).

[8] Banaszek, K., D'Ariano, G. M., Paris, M. G. A., & Sacchi, M. F. Maximum-likelihood estimation of the density matrix. Phys. Rev. A 61, 010304(R) (2000).

[9] White, A. G., James, D. F. V., Munro, W. J. & Kwiat, P. G. Exploring Hilbert Space: Accurate characterization of quantum information. Phys. Rev. A **65,** 012301 (2002).

[10] Ourjoumtsev, A., Jeong, H., Tualle-Brouri, R., & Grangier, P. Generation of optical 'Schrödinger cats' from photon number states. Nature **448,** 784 (2007).

[11] Neergaard-Nielsen, J. S., Melholt Nielsen, B., Hettich, C., Mølmer, K. & Polzik, E. S. Generation of a superposition of odd photon number states for quantum information networks. Phys. Rev. Lett. 97, 083604 (2006).

[12] Chuang, I. L. & Nielsen, M. A. Prescription for experimental determination of the dynamics of a quantum black box. J. Mod. Opt. **44,** 2455 (1997).

[13] Poyatos, J. F., Cirac, J. I. & Zoller, P. Complete characterization of a quantum process: The two-bit quantum gate. Phys. Rev. Lett. **78,** 390 (1997).

[14] D'Ariano, G. M. & Maccone, L. Measuring quantum optical Hamiltonians. Phys. Rev. Lett. **80,** 5465 (1998).

[15] Nielsen, M. A., Knill, E., & Laflamme, R. Complete quantum teleportation using nuclear magnetic resonance. Nature **396**, 52 (1998).

[16] Altepeter, J. B. et al. Ancilla-assisted quantum process tomography. Phys. Rev. Lett. **90,** 193601 (2003).

[17] Mitchell, M. W., Ellenor, C. W., Schneider, S. & Steinberg, A. M. Diagnosis, prescription and prognosis of a Bell-state filter by quantum process tomography. Phys. Rev. Lett. **91,** 120402 (2003).

[18] Achilles, D., Silberhorn, Ch., Sliwa, C., Banaszek, K., & Walmsley, I. A. Fiber-assisted detection with photon number resolution. Opt. Lett. **28,** 2387 (2003).

[19] Resch, K. J. et al. Time-reversal and super-resolving phase measurements. Phys. Rev. Lett. **98,** 223601 (2007).

[20] Higgins, B. L., Berry, D. W., Bartlett, S. D., Wiseman, H. M. & Pryde, G. J. Entanglement-free Heisenberg-limited phase estimation. Nature **450,** 393 (2007).

[21] Knill, E. and Laflamme, R. & Milburn, G. J., A scheme for efficient quantum computation with linear optics. Nature **409,** 46-52 (2001).

[22] Boyd, S. & Vandenberghe, L. *Convex optimization* (Cambridge Univ. Press, Cambridge, 2004).

[23] Lvovsky, A. I. et al. Quantum state reconstruction of the single-photon Fock state. Phys. Rev. Lett. **87,** 050402 (2001).

[24] Achilles, D. et al. Photon-number-resolving detection using time-multiplexing. J. Mod. Opt. **51,** 1499 (2004).

[25] Leonhardt, U. *Measuring the quantum state of light* (Cambridge Univ. Press, Cambridge, 1997).

[26] Eisert, J., Scheel, S., & Plenio, M. B. Distilling Gaussian states with Gaussian operations is impossible. Phys. Rev. Lett. **89,** 137903 (2002).

[27] Browne, D. E., Eisert, J., Scheel, S. & Plenio, M. B. Driving non-Gaussian to Gaussian states with linear optics. Phys. Rev. A **67,** 062320 (2003).

[28] Kardynal, B. E., Yuan, Z. L. & Shields, A. J. An avalanche-

photodiode-based photon-number-resolving detector. Nature Photonics advance online publication, 15 June 2008 (DOI 10.1038/nphoton.2008.101).

[29] Boulant, N., Havel, T. F., Pravia, M. A. & Cory, D. G. Robust method for estimating the Lindblad operators of a dissipative quantum process from measurements of the density operator at multiple time points. Phys. Rev. A **67**, 042322 (2003).

[30] Jezek, M., Fiurasek, J. & Hradil, Z. Quantum inference of states and processes. Phys. Rev. A **68**, 012305 (2003).